

Article

Surface Plasmon Resonance Induced Photocatalysis in 2D/2D Graphene/g-C₃N₄ Heterostructure for Enhanced Degradation of Amine-Based Pharmaceuticals under Solar Light Illumination

Faisal Al Marzouqi¹ and Rengaraj Selvaraj^{2,*}

¹ Department of Engineering, International Maritime College Oman, National University of Science and Technology, Falaj Al Qabail, P.O. Box 532, Suhar 322, Oman

² Department of Chemistry, College of Science, Sultan Qaboos University, Al-Khoudh, P.O. Box 36, Muscat 123, Oman

* Correspondence: rengaraj@squ.edu.om; Tel.: +968-2414-2436

Abstract: Pharmaceuticals, especially amine-based pharmaceuticals, such as nizatidine and ranitidine, contaminate water and resist water treatment. Here, different amounts of graphene sheets are coupled with g-C₃N₄ nanosheets (wt% ratio of 0.5, 1, 3 and 5 wt% of graphene) to verify the effect of surface plasmon resonance introduced to the g-C₃N₄ material. The synthesized materials were systematically examined by advanced analytical techniques. The prepared photocatalysts were used for the degradation of amine-based pharmaceuticals (nizatidine and ranitidine). The results show that by introducing only 3 wt% graphene to g-C₃N₄, the absorption ability in the visible and near-infrared regions dramatically enhanced. The absorption in the visible range was 50 times higher when compared to the pure sample. These absorption features suggest that the surfaces of the carbon nitride sheet are covered by the graphene nanosheet, which would effectively apply the LSPR properties for catalytic determinations. The enhancement in visible light absorption in the composite was confirmed by PL analysis, which showed greater inhibition of the electron-hole recombination process. The XRD showed a decrease in the (002) plan due to the presence of graphene, which prevents further stacking of carbon nitride layers. Accordingly, the Gr/g-C₃N₄ composite samples exhibited an enhancement in the photocatalytic performance, specifically for the 5% Gr/g-C₃N₄ sample, and close to 85% degradation was achieved within 20 min under solar irradiation. Therefore, applying the Gr/g-C₃N₄ for the degradation of a pharmaceutical can be taken into consideration as an alternative method for the removal of such pollutants during the water treatment process. This enhancement can be attributed to surface plasmon resonance-induced photocatalysis in a 2D/2D graphene/g-C₃N₄ heterostructure.

Keywords: amine-based pharmaceutical; graphene; g-C₃N₄; nizatidine; photocatalysts; solar irradiation



Citation: Al Marzouqi, F.; Selvaraj, R. Surface Plasmon Resonance Induced Photocatalysis in 2D/2D Graphene/g-C₃N₄ Heterostructure for Enhanced Degradation of Amine-Based Pharmaceuticals under Solar Light Illumination. *Catalysts* **2023**, *13*, 560. <https://doi.org/10.3390/catal13030560>

Academic Editors: Weilong Shi, Feng Guo, Xue Lin and Yuanzhi Hong

Received: 12 February 2023

Revised: 7 March 2023

Accepted: 8 March 2023

Published: 10 March 2023



Copyright: © 2023 by the authors. Licensee MDPI, Basel, Switzerland. This article is an open access article distributed under the terms and conditions of the Creative Commons Attribution (CC BY) license (<https://creativecommons.org/licenses/by/4.0/>).

1. Introduction

Protecting the environment from pollution and delivering a sufficient amount of energy is vital to maintain our natural life on earth. Scientists are considering all the possible ways to keep the environment at a suitable level where the energy is supplied from a green sustainable source [1,2]. One of the possible solutions to maintain the green energy demand with the minimum environmental condition are the engineering and synthesizing of artificial photocatalysts with super photocatalytic activities. This field has attracted a huge scientific interest, resulting in many commercial products based on this technology. The current achievements in semiconductor materials are state-of-the-art technology, which has been applied in several necessary fields [1]. For example, water decontamination, environmental remediation, hydrogen production, photosensitive sensing, energy harvesting and energy-storing devices are intensively investigating the new implementation of semiconductor materials [2–6]. One of the goals is to fully utilize the abundantly free solar

irradiation for driving significant chemical reactions for large-scale applications. There are numerous categories of semiconductor photocatalysts that have been investigated, such as oxynitrides, sulfides, oxides and metal-free semiconductors [7–9]. Free metal semiconductors are highly considered; graphitic carbon nitride ($g\text{-C}_3\text{N}_4$) has shown a new possible application in the photocatalytic field due to its compatible properties [10–13]. This property allows the synthesis of a visible active material with more accessible properties; based on that, a universal consideration has been provided to investigate this specific material.

Hence, the $g\text{-C}_3\text{N}_4$ materials demonstrated that they were suitable and compatible with energy and sustainability applications. A thorough review of the literature can give the readers a general idea about the conditions required to synthesize carbon nitride materials, which are relatively easy and faster compared to the synthesis of metal oxides and metal sulfides photocatalysts. In general, the carbon nitride samples can be obtained via the thermal polycondensation reaction (450–550 °C) of nitrogen-rich precursors in a semi-close system. So far, many precursors have been used as starting materials, such as cyanamide, dicyanamide, triazine, heptazine, melamine, urea, thiourea and so on. The most dominated one is melamine because the yield generated is much higher and the defect is less compared to other starting materials.

The research reported data present more and more understanding of the photocatalyst's material's methods of working. Therefore, the attention has been orientated to synthesizing narrow band gap semiconductors and efficient in visible light absorption, as opposed to what is commonly used, namely, materials with wide band gap photocatalysts, such as TiO_2 and ZnO [7,8]. The drawbacks of these traditional semiconductor-based photocatalysts are weak light absorption in the visible light region, toxicity, short-term stability and/or high material costs [9–12]. On the other hand, a polymeric semiconductor based on graphitic carbon nitride $g\text{-C}_3\text{N}_4$ has been investigated for water splitting under visible light irradiation. $g\text{-C}_3\text{N}_4$ has a band gap value of 2.7 eV, indicating its visible light response [14,15]. This semiconductor exhibits excellent needed properties, such as a 2D shape structure, suitable redox potential, low band gap, high thermal chemical stability and suitability for large-scale production from low-cost precursors, such as urea, thiourea and melamine [16–20].

The main limitation in using $g\text{-C}_3\text{N}_4$ material as a photocatalyst is the high recombination rate of photogenerated electrons and holes, which limits the photocatalytic efficiency. Thus, finding an appropriate way to overcome the stated problems is challenging. There are numerous methods used to enhance the photocatalytic activity. Coupling materials were used to approach the desired enhancement in photocatalytic performance, such as $\text{CdS}/g\text{-C}_3\text{N}_4$, $\text{TiO}_2/g\text{-C}_3\text{N}_4$ and $\text{ZnO}/g\text{-C}_3\text{N}_4$ [13–17]. On the other hand, an interesting approach is introducing a surface plasmon resonance (SPR) effect on the surface of the semiconductor material to enhance the electron-hole separation ability [21–30]. In a characteristic SPR phenomenon, the plasmonic electrons on the surface interact with the absorbed photons and oscillate on the surface of the metallic nanomaterials, resulting in an improvement of the local electromagnetic field and stimulating active electrons on the semiconductor, which leads to enhancement in the visible light response [18,20,21]. Primarily, noble metal nanoparticles like Au, Pt and Ag were used to introduce a localized surface plasmon resonance SPR to the surface of $g\text{-C}_3\text{N}_4$. However, noble metals are expensive and have a shallow surface interaction with the surface of the $g\text{-C}_3\text{N}_4$ material. On the other hand, graphene (Gr) is a more affordable non-metallic material and has a strong ability to introduce surface plasmon resonance similar to metallic particles [31–35].

Recent studies showed that 2D/2D stacking can provide a better interaction compared to 0D/2D and 1D/2D stacking structures. Graphene can provide strong 2D/2D stacking interaction with g-C₃N₄; therefore, Gr/g-C₃N₄ composite material is a very attractive catalyst from both experimental and theoretical aspects [24–26]. To date, only a few studies have demonstrated the synthesis of Gr/g-C₃N₄ composite material via different methods, such as hydrothermal, solvothermal, ionic-liquid and hydrolysis routes. Compared to these preparation methods, the thermal method dramatically reduces the experimental time and enhances the product purity [36–39]. The other methods are relatively long and require multiple steps to obtain the final product. The direct thermal method shows great potential in reducing the process time and steps. The advantage of combining carbon nitride with graphene is that both materials are chemically and thermally stable.

The reported Gr/g-C₃N₄ composite was mainly used for hydrogen evolution, lithium batteries and photocatalytic degradation of dyes. Currently, more research is oriented in the direction of wastewater and drinking water treatment from pharmaceuticals [40,41]. Amine-based pharmaceuticals, such as nizatidine and ranitidine, have garnered maximum researcher attention due to the ability of these compounds to generate toxic nitrogenous disinfection by-products, which are formed during the disinfection step. On the other hand, only a few studies have been performed in the area of photocatalytic degradation of amine-based pharmaceuticals as an alternative method for conventional wastewater treatment [42–45].

Herein, an easy direct thermal method for synthesizing 2D/2D Gr/g-C₃N₄ nanocomposite material is reported. The amount of Gr attached to the g-C₃N₄ sheets was investigated by varying the percentage of Gr from 0% up to 5% (pure g-C₃N₄, 0.5% Gr/g-C₃N₄, 1% Gr/g-C₃N₄, 3% Gr/g-C₃N₄ and 5% Gr/g-C₃N₄). Then, the effect of SPR on the g-C₃N₄ surface was examined. The photocatalytic performance of the photocatalysts was evaluated by the degradation of amine-based pharmaceuticals, nizatidine and ranitidine, under stable LED and direct solar light. The improvement in the visible light absorption in the combination was validated by optical and physical analyses, which showed superior inhibition of the electron-hole recombination process. Consequently, the Gr/g-C₃N₄ composite samples demonstrated a boost in the photocatalytic performance, specifically for the 5% Gr/g-C₃N₄ sample, and up to 85% degradation was achieved within 20 min under solar irradiation.

2. Results and Discussion

2.1. XRD Analysis

An X-ray diffraction analysis was performed to investigate the crystalline properties of the synthesized carbon nitride material. Figure 1 shows the XRD patterns of the Gr/g-C₃N₄ prepared via a direct thermal method. All the samples exhibited two main diffraction peaks. The first peak at around 27.90° corresponds to the (002) diffraction peaks characteristic of interlayer stacking of aromatic systems, and the second diffraction peak at around 13.05° is indexed to the (100) peak that represents inter-planar separation. These diffraction peaks are in good agreement with those reported for g-C₃N₄ and were retained during thermal oxidation [11,12], indicating the existence of the graphite-like structure of g-C₃N₄. The results show that increasing the amount of graphene amount reduces the diffraction peak 002. This kind of decrease in the 002 plan growth direction is expected. It can be attributed to the presence of graphene, which prevents further stacking of carbon nitride layers.

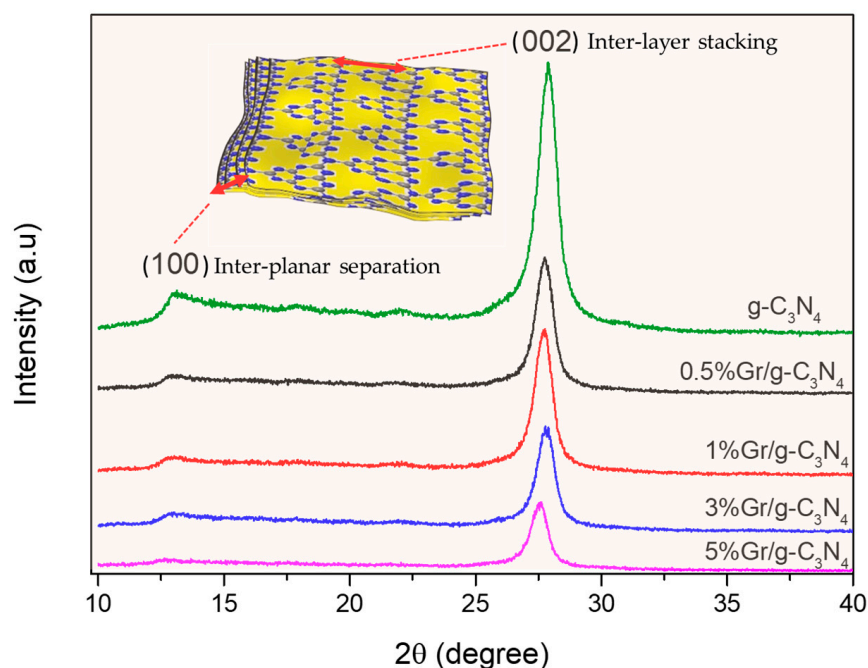


Figure 1. The XRD patterns of the Gr/g-C₃N₄ were prepared via the thermal method (inset schematic presentation of graphene stacking between g-C₃N₄ layers).

2.2. SEM, EDX and TEM Analysis

The morphological features of the Gr/g-C₃N₄ samples prepared via the direct heating method were determined by scanning electron microscopy (SEM). Figure 2 shows the SEM images of different percentages of the Gr/g-C₃N₄ samples. The g-C₃N₄ image depicted sheet-like microstructures. Moreover, the fabrication of g-C₃N₄ in the presence of graphene did not change the sheet structure of carbon nitride. The amount of graphene added to the surface of the g-C₃N₄ sheet was increased from 0.5% to 5%. However, the 2D/2D type of composite was expected to enhance the photocatalytic performance due to the higher area of interaction [24]. On the other hand, energy dispersive X-ray spectroscopy (EDXs) was also used to identify and confirm the elemental composition of the synthesized samples. The elemental composition of the prepared composite samples has been measured via EDXs analysis and the result is shown in Figure 3. It is seen that the sample was composed mainly of three main elements: carbon, nitrogen and oxygen. The atomic ratio of C:N was 56.9:38.5 wt%. These results further confirm the high purity of the produced Gr/g-C₃N₄ sample. To confirm the coupling of the graphene nanosheets and the carbon nitride nanosheets in a 2D/2D structure, a TEM analysis was carried out. Figure 4a shows the TEM image of the pure graphene sample. Figure 4b shows the TEM image of the Gr/g-C₃N₄ sample. High magnification on the selected area is presented in Figure 4c. The image clearly shows the presence of both sheets, indicating the formation of the Gr/g-C₃N₄ composite.

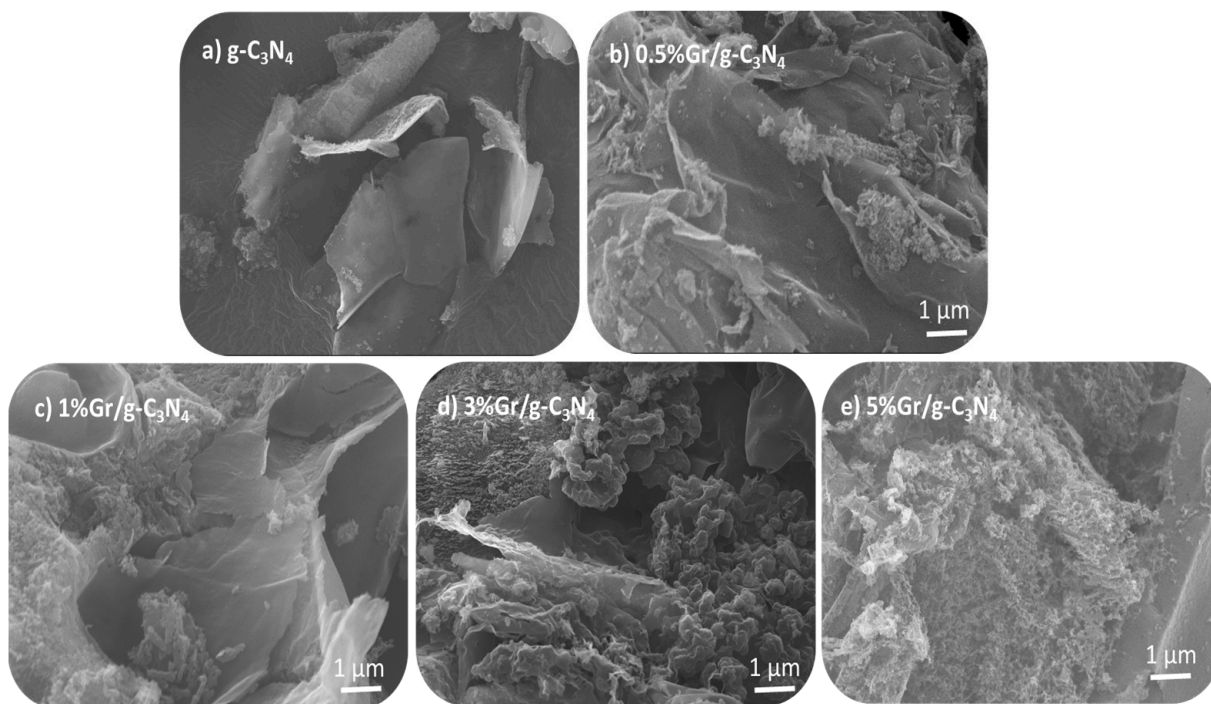


Figure 2. The SEM images of (a) g-C₃N₄, (b) 0.5%Gr/g-C₃N₄, (c) 1%Gr/g-C₃N₄, (d) 3%Gr/g-C₃N₄ and (e) 5%Gr/g-C₃N₄ samples.

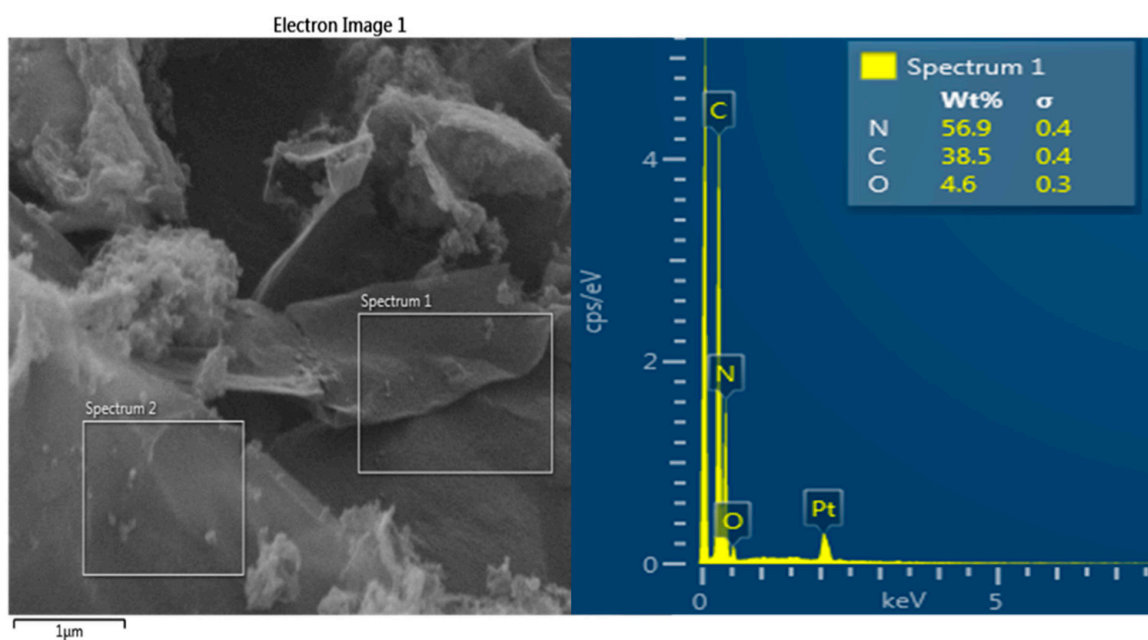


Figure 3. The element's presence in the Gr/g-C₃N₄ sample.

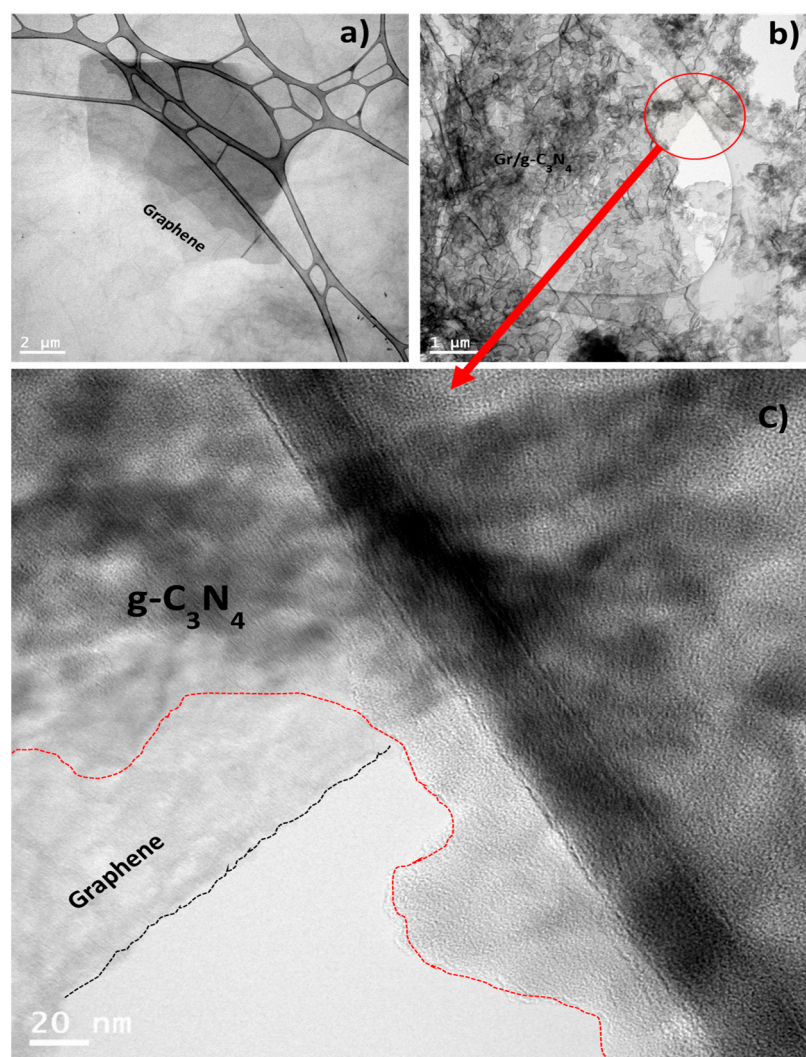


Figure 4. TEM images of (a) the graphene sheet, (b) the Gr/g-C₃N₄ composite samples and (c) high resolution of a selected area (red arrow) of the Gr/g-C₃N₄ composite.

2.3. UV-DRS Analysis

The UV-Vis diffuse reflectance spectra (UV-DRS) were used to investigate the optical properties of the as-prepared photocatalysts (Figure 5). In general, the absorbance spectra of direct inter-band transition energies of the prepared material are located at the edge of the visible region, which is compatible with the small band gap energy (2.7 eV). The UV diffuse reflectance spectrum of the synthesized samples is shown in Figure 5a. The fundamental absorption edge of the g-C₃N₄ material was about 450 nm, which is considered to be in the visible light range. Moreover, the coupling of g-C₃N₄ with graphene showed a small red shift of the band edge, which is expected to enhance the photocatalytic performance of the heterostructure. The optical band gap was calculated according to the following Tauc equation (Equation (1)):

$$\alpha h\nu = A(h\nu - E_g)^{n/2} \quad (1)$$

where α , ν , A and E_g are the absorption coefficient, light frequency, proportionality constant and band gap, respectively. The band gap energy is obtained from the slope drawn near the band edge. The band gap values for g-C₃N₄, 0.5%Gr/g-C₃N₄, 1%Gr/g-C₃N₄, 3%Gr/g-C₃N₄ and 5%Gr/g-C₃N₄ samples were 2.76, 2.75, 2.72, 2.73 and 2.73 eV, respectively (Figure 5b–f). The small changes observed in the band gap were expected because the main role of graphene is to facilitate the separation of charge carriers. Moreover, increasing the amount of graphene ends up elevating the absorption tail due to the plasmonic effect of

free electrons on the surface of the graphene [22,23]. The addition of 3% and 5% graphene on the $g\text{-C}_3\text{N}_4$ structure enhanced the absorption in the visible range by 50 times when compared to the pure sample. These absorption features suggest that the surfaces of the carbon nitride sheet are covered by the graphene nanosheet, which would effectively apply the LSPR properties for catalytic determinations.

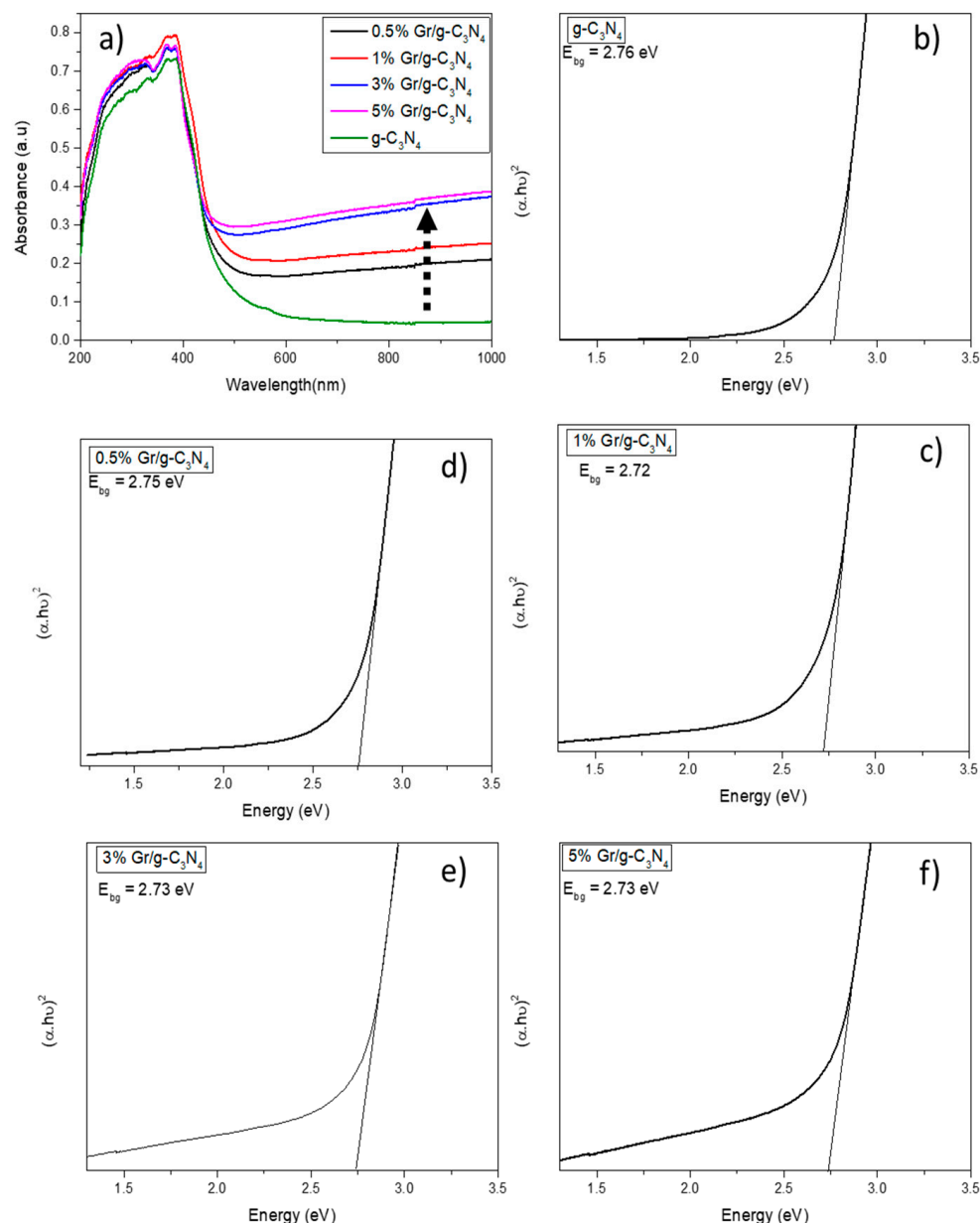


Figure 5. (a) UV diffuse reflectance spectra of the obtained samples; (b–f) the corresponding Tauc plot of the samples.

2.4. Photoluminescence Analysis (PL)

The photoluminescence emission peak is mainly considered a result of the recombination process of the photo-generated electrons and hole pairs. In general, the photoluminescence emission peak intensity is higher, indicating a higher recombination rate for photo-generated electrons and holes [34]. Figure 6a shows the PL emission spectra of the $g\text{-C}_3\text{N}_4$ and Gr/ $g\text{-C}_3\text{N}_4$ composite samples. All the samples were exposed to an excitation process at a wavelength of 370 nm at room temperature and the main emission peak is observed at about 450 nm. The PL intensities of $g\text{-C}_3\text{N}_4$ reduced dramatically after coupling $g\text{-C}_3\text{N}_4$ with graphene, indicating the inhabitation of the recombination process

of free charge carriers in the composite samples. Moreover, the 5% Gr/g-C₃N₄ has the lowest PL peak intensity compared to the other samples. The Gaussian fitting was used to convolute the photoluminescence peaks, as shown in Figure 6a, which helps us to obtain a clear understanding of excitons in the Gr/g-C₃N₄ samples and the origin of the emission concerning the initial precursors. All the samples showed three emission peaks. The carbon nitride materials are expected to have three states formed due to the presence of the sp³ C-Nσ band, sp² C-Nπ band and the lone pair (LP) state of the bridge nitride atom [35,36]. To confirm the PL shift, the Commission Internationale de l'Éclairage (CIE) chromaticity diagram of the pure g-C₃N₄ sample and the Gr/g-C₃N₄ composite sample is presented in Figure 6b. The CIE (x, y) coordinate of the pure g-C₃N₄ samples located at (0.17, 0.18) were the CIE (x, y) coordinate of the Gr/g-C₃N₄ composite located at (0.19, 0.19), which further confirm that the PL emission is shifted toward light blue-violet. This further confirms that the PL emission is covering the blue-violet to close green light region. Additionally, the emission of carbon nitride products obtained from 5% graphene is located close to the edge of the blue-violet region, whereas the sample obtained from pure carbon nitride showed deep blue-violet. The differences in the colours further confirms the enhancement in visible light absorbance.

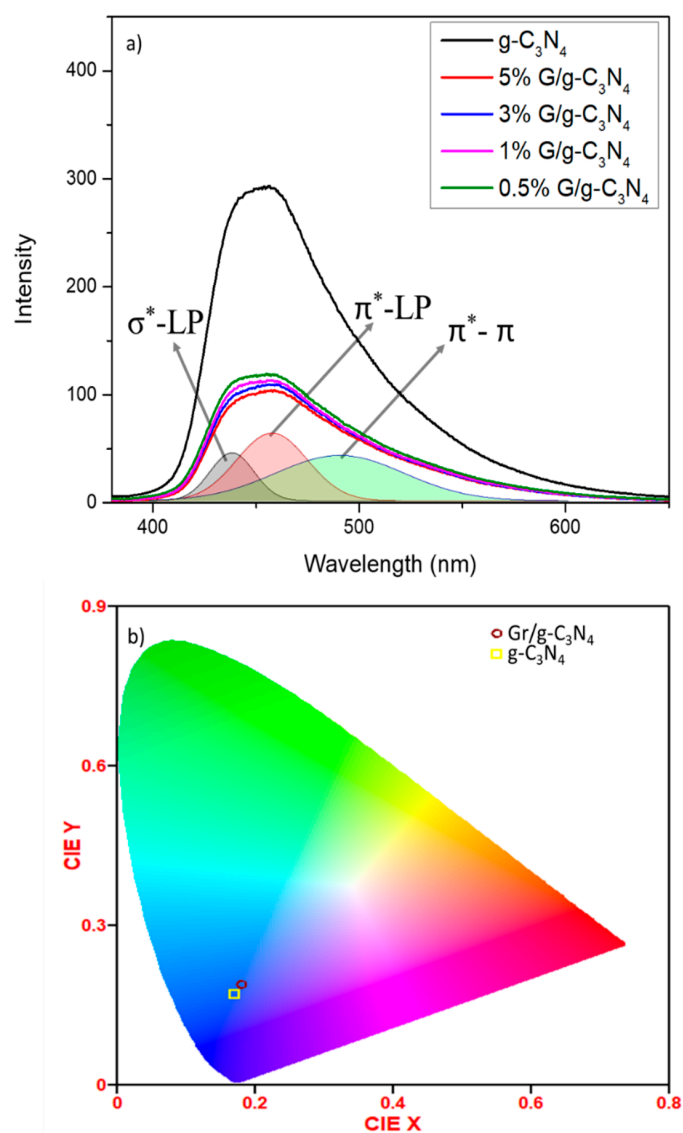


Figure 6. (a) The PL emission spectra of the prepared samples; (b) the (CIE) chromaticity diagram of the pure g-C₃N₄ sample and the Gr/g-C₃N₄ composite.

2.5. FTIR Analysis

The overlay FTIR spectra were measured to identify the characteristic peaks of the prepared samples. The response was recorded for the samples at the wavelength range of 600 to 4000 cm^{-1} . In general, all the samples demonstrate their graphitic structure, which can normally be shown as three main regions. Figure 7a shows the Fourier transform infrared (FTIR) spectrum of the as-prepared samples to identify the specific interaction of the functional groups. The result indicates the presence of the graphite-like structure of carbon nitride. The N-H stretching modes and the O-H from water absorbed on the surface are present in the broad peak observed in the range of 3000–3500 cm^{-1} . The bands around 1200–1600 cm^{-1} are characteristic of a typical stretching mode of CN heterocycles. In addition, the s-triazazine ring mode was observed at 801 cm^{-1} . However, there was some broadening in the peak at 3000–3500 cm^{-1} , which is indexed to CO vibration. One of the interesting properties that carbon nitride has is a surface of multiple functional groups, as presented in Figure 7b. These groups influence the behaviors of the prepared materials. The most common functional groups that appear while the preparation of carbon nitride is primary are secondary amine groups (CNH_2 and C_2NH) due to a small amount of hydrogen remaining from the initial precursor. The presence of an amine group makes carbon nitride exhibit electron-rich properties with basic behaviors and the ability for H-bonding motifs formation [11,12]. This impurity makes carbon nitride more applicable as catalysis compared to perfect and defect-free $\text{g-C}_3\text{N}_4$. This amine group makes carbon nitride materials more suitable for the removal of acidic toxic compounds via chemical adsorption on the surface with the help of electrostatic interactions.

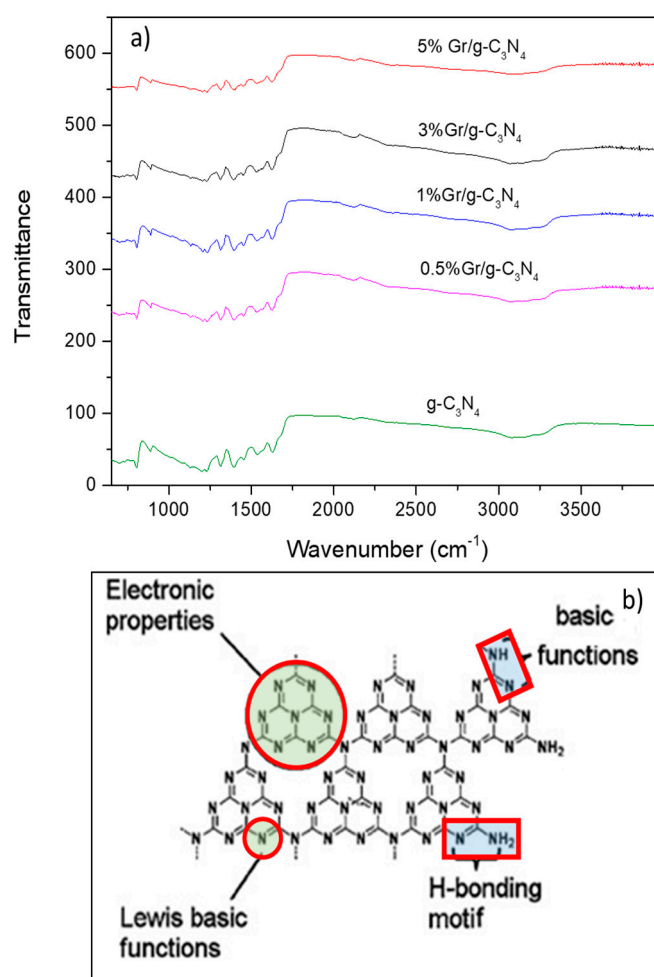


Figure 7. (a) FTIR spectrum of the $\text{g-C}_3\text{N}_4$ samples; (b) the functional groups on $\text{g-C}_3\text{N}_4$.

2.6. Photocatalytic Activity Test

The degradation of pharmaceuticals using the obtained Gr/g-C₃N₄ composite samples by the direct heating method was investigated under visible light and under direct solar light irradiation. The degradation of the selected pharmaceutical compounds was followed with the help of a UV spectrophotometer. The maximum absorbance peak for nizatidine and ranitidine was the same and was located at 312 nm (λ_{\max}). Figure 8a represents the concentration changes of nizatidine starting from an initial concentration of 5 mg/L of the nizatidine aqueous solution at pH = 5.6 (with 5% Gr/g-C₃N₄). Figure 8b represents the concentration changes of ranitidine starting at the same concentration. Moreover, a control experiment was carried out to verify the effect of the visible light on the pure g-C₃N₄. The initial concentration remained almost the same for the pure sample, indicating that the g-C₃N₄ by itself is not very active under this condition. However, the degradation was dramatically enhanced after the addition of the prepared Gr/g-C₃N₄ catalysts. All the prepared composite samples showed higher degradation performance. As expected, the Gr/g-C₃N₄ composite samples exhibited superior photocatalytic performance compared to the pure sample. The 5% Gr/g-C₃N₄ showed the best performance among all the prepared samples (see Figure 8c,d). The enhancement noticed for the 5% Gr/g-C₃N₄ sample could be attributed to the coupling of two materials, which facilitates an effective separation of the charge carriers, as shown in the UVDRS and PL results. Finally, the best sample was chosen to be tested under direct solar light irradiation (Figure 9a). The sample showed more enhanced performance under solar irradiation due to more light intensity, more than 80% degradation achieved within 20 min. Figure 9b shows a schematic presentation of the charge carrier formation and the mechanism of the degradation.

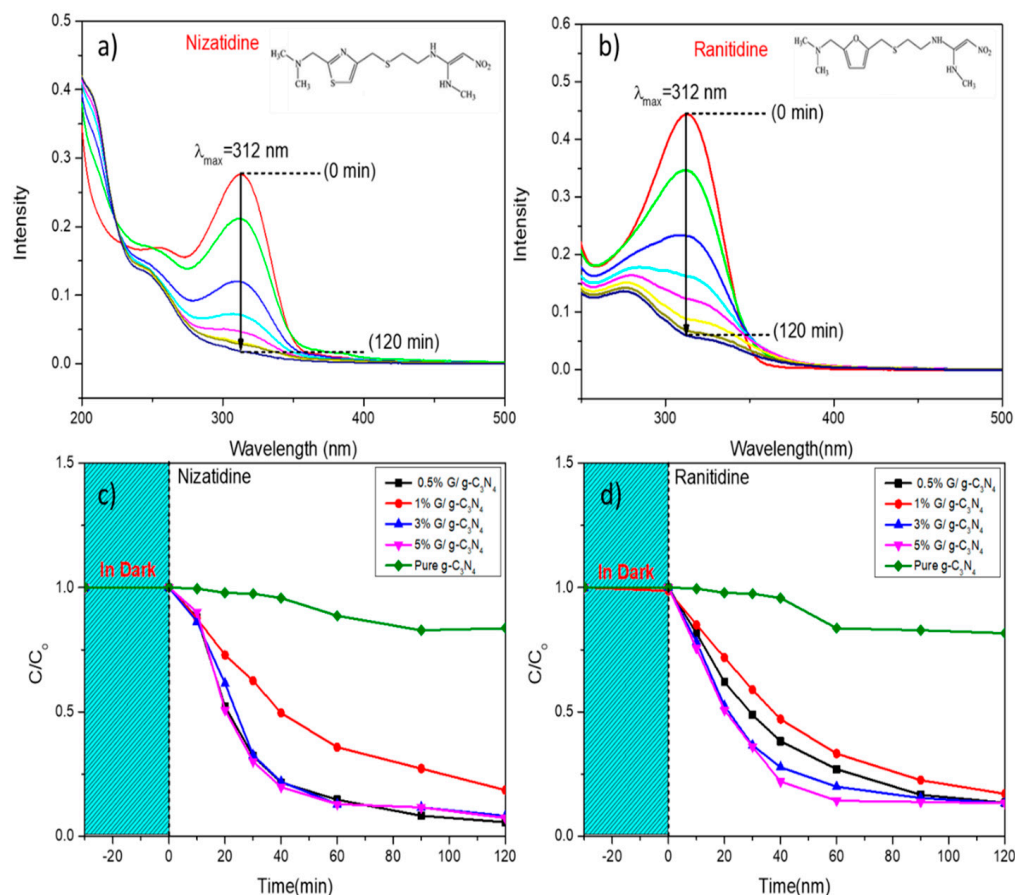


Figure 8. (a) The degradation rate of nizatidine and (b) ranitidine at an initial concentration of 5 mg/L and pH = 5.6 with 5% Gr/g-C₃N₄. (c,d) C/C_0 Plots for nizatidine and ranitidine, respectively, under UV irradiation.

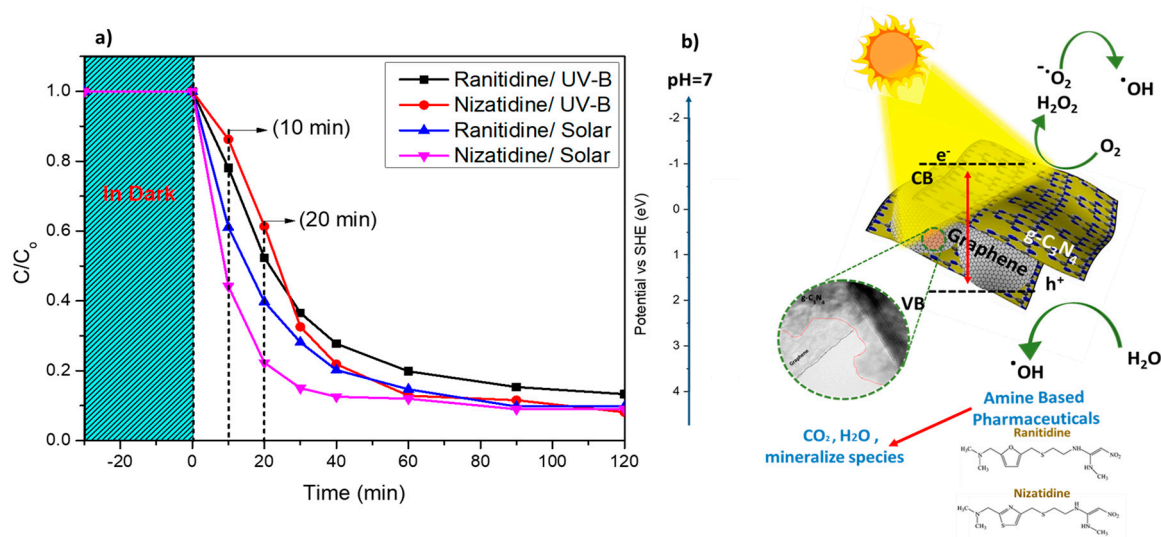


Figure 9. (a) C/C_0 Plots for nizatidine and ranitidine under UV and Solar irradiation. (b) the photocatalytic mechanism under solar light.

3. Materials and Methods

3.1. Materials

The melamine powder (M2659 Aldrich, St. Louis, MO, USA) and graphene oxide (763705-100 ML, St. Louis, MO, USA) were purchased from Sigma-Aldrich and were used without further purification.

3.2. Characterization

The prepared samples were examined by an X-ray diffraction (XRD, Malvern, UK) test using an XRD Panalytical X-pert Pro instrument equipped with graphite monochromatized Cu K α radiation ($\lambda = 1.540 \text{ \AA}$). The detector was NaI (T1). The samples' morphologies were observed using a field emission scanning electron microscope (FESEM, JSM-7800F JOEL, Tokyo, Japan) with a maximum working voltage of 30 kV, a maximum resolution of 0.8 nm and a working distance of 10 mm used during measurements where the elements were present near the surface, and analyzed by energy dispersive X-ray spectroscopy (EDX, JOEL, Tokyo, Japan). The transmission electron microscope (TEM, JOEL, Tokyo, Japan) model JEM-1400-JEOL was used for high-resolution analysis. The UV-Vis diffuse reflection spectroscopy (UV-Vis DRS, Waltham, MA, USA) measurements were conducted using the Perkin Elmer Lambda 650S spectrometer. The photoluminescence (PL, Waltham, MA, USA) behavior was evaluated using a Perkin-Elmer LS 55 Luminescence Spectrometer. The degradation of amine-based pharmaceuticals (nizatidine and ranitidine) was analyzed by a Shimadzu UV-1800 UV/Visible Scanning Spectrophotometer (Shimadzu, Kyoto, Japan).

3.3. Synthesis of Gr/g- C_3N_4 Composite Materials

The graphene (Gr)-based carbon nitride materials (g- C_3N_4) were prepared by mixing a specific volume of a graphene oxide solution with melamine powder. One gram of melamine powder was mixed with the required wt% ratio of 0.5, 1, 3 and 5 wt% of graphene, then placed in an alumina crucible and covered with a lid. The mixture of the graphene oxide and melamine powder was left to dry overnight in an air oven at 80 °C. The dried sample was crushed to a fine powder to ensure a homogeneous distribution of graphene in the mixture. Then, direct thermal heating was applied up to 550 °C at a heating rate of 20 °C/min and stabilized at 550 °C for 3 h. After cooling, the product was collected for further analysis and the process was repeated to obtain the required amount. Simplified schematic steps of the synthesis are presented in Figure 10. There was no further washing or purification performed. A pure carbon nitride sample was obtained by the same method without graphene added to the melamine powder.

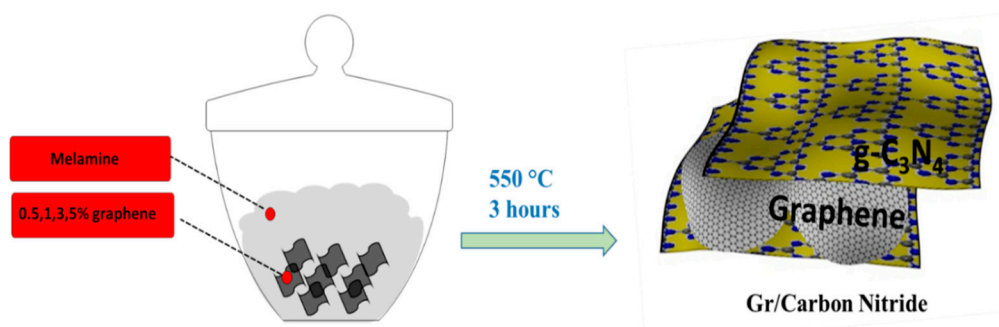


Figure 10. Schematic steps of the synthesis of Gr/g-C₃N₄.

3.4. Photocatalytic Test of (Gr/g-C₃N₄)

The photocatalytic activity performances of the as-prepared nanosheet were measured by following the degradation of two amine-based pharmaceutical compounds (nizatidine and ranitidine). The photoreaction analyses were conducted using a batch system reactor involving a cylindrical borosilicate glass vessel with an effective volume of 500 mL. All photoreaction was performed in an open atmosphere at a stable temperature (25 °C) with a cold water circulation system. The reactor was attached to an air diffuser machine to uniformly disperse the air into the solution. The suspensions (catalyst and pollutant solution) were prepared by adding 0.1 g of the prepared Gr/g-C₃N₄ powder into 250 mL of an aqueous solution of a nizatidine- and ranitidine-contaminated solution with an initial concentration of 5 mg/L (5 ppm). The system was chosen to be conducted in an open atmosphere with an air diffuser fixed at the reactor to mimic a real-life situation and uniformly disperse the air into the solution. The reaction suspensions were magnetically stirred for 30 min in the dark to ensure adsorption–desorption equilibrium between the photocatalyst and the pharmaceuticals. One sample was taken after this step to evaluate the adsorption amount. During illumination with light, about 6 mL of the suspension solution was taken from the reactor at a scheduled interval. The samples were filtered to remove the catalyst. For a stable UV source of light, a Mic-LED-365 (from Prizmatix 420 mW) was used to activate the photocatalytic reaction, then the experiment was repeated under direct solar irradiation with an average intensity in the range of 1100–1300 W/m².

4. Conclusions

In conclusion, the Gr/g-C₃N₄ composite photocatalytic materials were successfully synthesized by the direct thermal method and were demonstrated to be a highly competitive catalytic system with superior activity for visible-light-induced degradation of amine-based pharmaceuticals (nizatidine and ranitidine). The results from X-ray diffraction, the samples' morphologies and the surface analyzed by energy dispersive X-ray spectroscopy (EDX) and PL indicate that the selected method can simplify the preparation of Gr/g-C₃N₄ compared to other techniques. The photocatalytic tests of the prepared Gr/g-C₃N₄ samples showed higher efficiency for the degradation of amine-based pharmaceutical models under solar light irradiation. The sample with a 5% graphene to g-C₃N₄ ratio showed the highest photocatalytic activity compared to lower graphene percentages (0.5%, 1%, 2% and 3%). The degradation reached 85% within only 20 min. Therefore, applying Gr/g-C₃N₄ for the degradation of a pharmaceutical can be taken into consideration as an alternative method for the removal of such pollutants during the water treatment process. This enhancement can be attributed to surface plasmon resonance-induced photocatalysis in a 2D/2D graphene/g-C₃N₄ heterostructure. Thus, 2D/2D graphene/g-C₃N₄ heterostructures can be useful materials for the removal of pharmaceutical pollutants from water using solar energy.

Author Contributions: Methodology, R.S.; formal analysis, F.A.M.; investigation, F.A.M.; writing—original draft preparation, F.A.M.; writing—review and editing, R.S.; supervision, R.S.; project administration, R.S.; funding acquisition, R.S. All authors have read and agreed to the published version of the manuscript.

Funding: This research received no external funding.

Data Availability Statement: The data presented in this study are available on request from the corresponding author. The data are not publicly available due to the nature of the data.

Acknowledgments: Faisal Al Marzouqi wishes to thank the International Maritime College Oman, Sultanate of Oman for the support (2022/CRG 09). Rengaraj Selvaraj acknowledges the Surface Science Lab, Department of Physics, College of Science, Sultan Qaboos University and The Central Analytical and Applied Research Unit (CAARU) College of Science, Sultan Qaboos University, Oman.

Conflicts of Interest: The authors declare no conflict of interest.

References

1. Ahmad, R.; Ahmad, Z.; Khan, A.U.; Mastoi, N.R.; Aslam, M.; Kim, J. Photocatalytic systems as an advanced environmental remediation: Recent developments, limitations and new avenues for applications. *J. Environ. Chem. Eng.* **2016**, *4*, 4143–4164. [[CrossRef](#)]
2. Al Balushi, B.S.; Al Marzouqi, F.; Al Wahaibi, B.; Kuvarega, A.T.; Al Kindy, S.M.; Kim, Y.; Selvaraj, R. Hydrothermal synthesis of CdS sub-microspheres for photocatalytic degradation of pharmaceuticals. *Appl. Surf. Sci.* **2018**, *457*, 559–565. [[CrossRef](#)]
3. Chen, X.; Shen, S.; Guo, L.; Mao, S.S. Semiconductor-based photocatalytic hydrogen generation. *Chem. Rev.* **2010**, *110*, 6503–6570. [[CrossRef](#)] [[PubMed](#)]
4. Fresno, F.; Portela, R.; Suárez, S.; Coronado, J.M. Photocatalytic materials: Recent achievements and near future trends. *J. Mater. Chem. A* **2014**, *2*, 2863–2884. [[CrossRef](#)]
5. Liu, J.; Zhang, Y.; Lu, L.; Wu, G.; Chen, W. Self-regenerated solar-driven photocatalytic water-splitting by urea derived graphitic carbon nitride with platinum nanoparticles. *Chem. Commun.* **2012**, *48*, 8826–8828. [[CrossRef](#)]
6. Tauc, J.; Grigorovici, R.; Vancu, A. Optical properties and electronic structure of amorphous germanium. *Phys. Status Solidi B* **1966**, *15*, 627–637. [[CrossRef](#)]
7. Al Marzouqi, F.; Al-Balushi, N.A.; Kuvarega, A.T.; Karthikeyan, S.; Selvaraj, R. Thermal and hydrothermal synthesis of WO₃ nanostructure and its optical and photocatalytic properties for the degradation of Cephalexin and Nizatidine in aqueous solution. *Mater. Sci. Eng. B* **2021**, *264*, 114991. [[CrossRef](#)]
8. Al Sarihi, F.T.; Al Marzouqi, F.; Kuvarega, A.T.; Karthikeyan, S.; Selvaraj, R. Easy conversion of BiOCl plates to flowers like structure to enhance the photocatalytic degradation of endocrine disrupting compounds. *Mater. Res. Express* **2020**, *6*, 125537. [[CrossRef](#)]
9. Meetani, M.A.; Alaidaros, A.; Hisaindee, S.; Alhamadat, A.; Selvaraj, R.; Al Marzouqi, F.; Rauf, M.A. Photocatalytic degradation of acetaminophen in aqueous solution by Zn-0.2 Cd_{0.8}S catalyst and visible radiation. *Desalination Water Treat.* **2019**, *138*, 270–279. [[CrossRef](#)]
10. Al Marzouqi, F.; Kim, Y.; Selvaraj, R. Shifting of the band edge and investigation of charge carrier pathways in the CdS/g-C₃N₄ heterostructure for enhanced photocatalytic degradation of levofloxacin. *New J. Chem.* **2019**, *43*, 9784–9792. [[CrossRef](#)]
11. Al Marzouqi, F.; Selvaraj, R.; Kim, Y. Thermal oxidation etching process of g-C₃N₄ nanosheets from their bulk materials and its photocatalytic activity under solar light irradiation. *Desalination Water Treat.* **2018**, *116*, 267–276. [[CrossRef](#)]
12. Al Marzouqi, F.; Selvaraj, R.; Kim, Y. Rapid photocatalytic degradation of acetaminophen and levofloxacin using g-C₃N₄ nanosheets under solar light irradiation. *Mater. Res. Express* **2020**, *6*, 125538. [[CrossRef](#)]
13. Bai, Y.; Chen, T.; Wang, P.; Wang, L.; Ye, L.; Shi, X.; Bai, W. Size-dependent role of gold in g-C₃N₄/BiOBr/Au system for photocatalytic CO₂ reduction and dye degradation. *Sol. Energy Mater. Sol. Cells* **2016**, *157*, 406–414. [[CrossRef](#)]
14. Cheng, F.; Yin, H.; Xiang, Q. Low-temperature solid-state preparation of ternary CdS/g-C₃N₄/CuS nanocomposites for enhanced visible-light photocatalytic H₂-production activity. *Appl. Surf. Sci.* **2017**, *391*, 432–439. [[CrossRef](#)]
15. He, Y.; Wang, Y.; Zhang, L.; Teng, B.; Fan, M. High-efficiency conversion of CO₂ to fuel over ZnO/g-C₃N₄ photocatalyst. *Appl. Catal. B Environ.* **2015**, *168*, 1–8. [[CrossRef](#)]
16. Li, K.; Gao, S.; Wang, Q.; Xu, H.; Wang, Z.; Huang, B.; Dai, Y.; Lu, J. In-situ-reduced synthesis of Ti³⁺ self-doped TiO₂/g-C₃N₄ heterojunctions with high photocatalytic performance under LED light irradiation. *ACS Appl. Mater. Interfaces* **2015**, *7*, 9023–9030. [[CrossRef](#)]
17. Al Marzouqi, F.; Al Farsi, B.; Kuvarega, A.T.; Al Lawati, H.A.; Al Kindy, S.M.; Kim, Y.; Selvaraj, R. Controlled Microwave-Assisted Synthesis of the 2D-BiOCl/2D-g-C₃N₄ Heterostructure for the Degradation of Amine-Based Pharmaceuticals under Solar Light Illumination. *ACS Omega* **2019**, *4*, 4671–4678. [[CrossRef](#)]
18. Li, H.; Jing, Y.; Ma, X.; Liu, T.; Yang, L.; Liu, B.; Yin, S.; Wei, Y.; Wang, Y. Construction of a well-dispersed Ag/graphene-like gC₃N₄ photocatalyst and enhanced visible light photocatalytic activity. *RSC Adv.* **2017**, *7*, 8688–8693. [[CrossRef](#)]

19. Peng, B.; Tang, L.; Zeng, G.; Fang, S.; Ouyang, X.; Long, B.; Zhou, Y.; Deng, Y.; Liu, Y.; Wang, J. Self-powered photoelectrochemical aptasensor based on phosphorus doped porous ultrathin g-C₃N₄ nanosheets enhanced by surface plasmon resonance effect. *Biosens. Bioelectron.* **2018**, *121*, 19–26. [[CrossRef](#)]
20. Tonda, S.; Kumar, S.; Shanker, V. Surface plasmon resonance-induced photocatalysis by Au nanoparticles decorated mesoporous g-C₃N₄ nanosheets under direct sunlight irradiation. *Mater. Res. Bull.* **2016**, *75*, 51–58. [[CrossRef](#)]
21. Wang, H.; Sun, T.; Chang, L.; Nie, P.; Zhang, X.; Zhao, C.; Xue, X. The g-C₃N₄ nanosheets decorated by plasmonic Au nanoparticles: A heterogeneous electrocatalyst for oxygen evolution reaction enhanced by sunlight illumination. *Electrochim. Acta* **2019**, *303*, 110–117. [[CrossRef](#)]
22. Farmani, A.; Mir, A. Graphene sensor based on surface plasmon resonance for optical scanning. *IEEE Photonics Technol. Lett.* **2019**, *31*, 643–646. [[CrossRef](#)]
23. Islam, M.; Sultana, J.; Biabanifard, M.; Vafapour, Z.; Nine, M.; Dinovitser, A.; Cordeiro, C.; Ng, B.-H.; Abbott, D. Tunable localized surface plasmon graphene metasurface for multiband superabsorption and terahertz sensing. *Carbon* **2020**, *158*, 559–567. [[CrossRef](#)]
24. Ji, M.; Di, J.; Ge, Y.; Xia, J.; Li, H. 2D-2D stacking of graphene-like g-C₃N₄/Ultrathin Bi₄O₅Br₂ with matched energy band structure towards antibiotic removal. *Appl. Surf. Sci.* **2017**, *413*, 372–380. [[CrossRef](#)]
25. Liu, W.; Qiao, L.; Zhu, A.; Liu, Y.; Pan, J. Constructing 2D BiOCl/C₃N₄ layered composite with large contact surface for visible-light-driven photocatalytic degradation. *Appl. Surf. Sci.* **2017**, *426*, 897–905. [[CrossRef](#)]
26. Wang, Q.; Wang, W.; Zhong, L.; Liu, D.; Cao, X.; Cui, F. Oxygen vacancy-rich 2D/2D BiOCl-g-C₃N₄ ultrathin heterostructure nanosheets for enhanced visible-light-driven photocatalytic activity in environmental remediation. *Appl. Catal. B Environ.* **2018**, *220*, 290–302. [[CrossRef](#)]
27. Tompsett, G.A.; Conner, W.C.; Yngvesson, K.S. Microwave synthesis of nanoporous materials. *Chemphyschem* **2006**, *7*, 296–319. [[CrossRef](#)]
28. Pu, X.; Zhang, D.; Gao, Y.; Shao, X.; Ding, G.; Li, S.; Zhao, S. One-pot microwave-assisted combustion synthesis of graphene oxide-TiO₂ hybrids for photodegradation of methyl orange. *J. Alloys Compd.* **2013**, *551*, 382–388. [[CrossRef](#)]
29. Cruz, M.; Gomez, C.; Duran-Valle, C.J.; Pastrana-Martínez, L.M.; Faria, J.L.; Silva, A.M.; Faraldos, M.; Bahamonde, A. Bare TiO₂ and graphene oxide TiO₂ photocatalysts on the degradation of selected pesticides and influence of the water matrix. *Appl. Surf. Sci.* **2017**, *416*, 1013–1021. [[CrossRef](#)]
30. Harish, S.; Archana, J.; Sabarinathan, M.; Navaneethan, M.; Nisha, K.; Ponnusamy, S.; Muthamizhchelvan, C.; Ikeda, H.; Aswal, D.; Hayakawa, Y. Controlled structural and compositional characteristic of visible light active ZnO/CuO photocatalyst for the degradation of organic pollutant. *Appl. Surf. Sci.* **2017**, *418*, 103–112. [[CrossRef](#)]
31. Bing, J.; Hu, C.; Zhang, L. Enhanced mineralization of pharmaceuticals by surface oxidation over mesoporous γ -Ti-Al₂O₃ suspension with ozone. *Appl. Catal. B Environ.* **2017**, *202*, 118–126. [[CrossRef](#)]
32. Liu, C.; Wang, J.; Chen, W.; Dong, C.; Li, C. The removal of DON derived from algae cells by Cu-doped TiO₂ under sunlight irradiation. *Chem. Eng. J.* **2015**, *280*, 588–596. [[CrossRef](#)]
33. Sharma, A.; Ahmad, J.; Flora, S. Application of advanced oxidation processes and toxicity assessment of transformation products. *Environ. Res.* **2018**, *167*, 223–233. [[CrossRef](#)] [[PubMed](#)]
34. Wen, J.; Xie, J.; Chen, X.; Li, X. A review on g-C₃N₄-based photocatalysts. *Appl. Surf. Sci.* **2017**, *391*, 72–123. [[CrossRef](#)]
35. Dong, G.; Zhang, Y.; Pan, Q.; Qiu, J. A fantastic graphitic carbon nitride (g-C₃N₄) material: Electronic structure, photocatalytic and photoelectronic properties. *J. Photochem. Photobiol. C Photochem. Rev.* **2014**, *20*, 33–50. [[CrossRef](#)]
36. Xu, J.; Shalom, M.; Piersimoni, F.; Antonietti, M.; Neher, D.; Brenner, T.J. Color-Tunable Photoluminescence and NIR Electroluminescence in Carbon Nitride Thin Films and Light-Emitting Diodes. *Adv. Opt. Mater.* **2015**, *3*, 913–917. [[CrossRef](#)]
37. Liang, Z.; Xue, Y.; Wang, X.; Zhang, X.; Tian, J. Structure engineering of 1T/2H multiphase MoS₂ via oxygen incorporation over 2D layered porous g-C₃N₄ for remarkably enhanced photocatalytic hydrogen evolution. *Mater. Today Nano* **2022**, *18*, 100204. [[CrossRef](#)]
38. Fang, B.; Xing, Z.; Sun, D.; Li, Z.; Zhou, W. Hollow semiconductor photocatalysts for solar energy conversion. *Adv. Powder Mater.* **2022**, *1*, 100021. [[CrossRef](#)]
39. Liu, X.; Han, X.; Liang, Z.; Xue, Y.; Zhou, Y.; Zhang, X.; Cui, H.; Tian, J. Phosphorous-doped 1T-MoS₂ decorated nitrogen-doped g-C₃N₄ nanosheets for enhanced photocatalytic nitrogen fixation. *J. Colloid Interface Sci.* **2022**, *605*, 320–329. [[CrossRef](#)]
40. Wang, C.; Liu, K.; Wang, D.; Wang, G.; Chu, P.K.; Meng, Z.; Wang, X. Hierarchical CuO-ZnO/SiO₂ fibrous membranes for efficient removal of congo red and 4-nitrophenol from water. *Adv. Fiber Mater.* **2022**, *4*, 1069–1080. [[CrossRef](#)]
41. Wang, Y.; Li, Z.; Fu, W.; Sun, Y.; Dai, Y. Core-Sheath CeO₂/SiO₂ Nanofibers as Nanoreactors for Stabilizing Sinter-Resistant Pt, Enhanced Catalytic Oxidation and Water Remediation. *Adv. Fiber Mater.* **2022**, *4*, 1278–1289. [[CrossRef](#)]
42. Li, M.; Chen, X.; Li, X.; Dong, J.; Zhao, X.; Zhang, Q. Controllable strong and ultralight aramid nanofiber-based aerogel fibers for thermal insulation applications. *Adv. Fiber Mater.* **2022**, *4*, 1267–1277. [[CrossRef](#)]
43. Li, S.; Wang, C.; Liu, Y.; Liu, Y.; Cai, M.; Zhao, W.; Duan, X. S-scheme MIL-101 (Fe) octahedrons modified Bi₂WO₆ microspheres for photocatalytic decontamination of Cr (VI) and tetracycline hydrochloride: Synergistic insights, reaction pathways, and toxicity analysis. *Chem. Eng. J.* **2023**, *455*, 140943. [[CrossRef](#)]

44. Cai, M.; Liu, Y.; Wang, C.; Lin, W.; Li, S. Novel Cd_{0.5}Zn_{0.5}S/Bi₂MoO₆ S-scheme heterojunction for boosting the photodegradation of antibiotic enrofloxacin: Degradation pathway, mechanism and toxicity assessment. *Sep. Purif. Technol.* **2023**, *304*, 122401. [[CrossRef](#)]
45. Andreou, E.K.; Koutsouroubi, E.D.; Vamvasakis, I.; Armatas, G.S. Ni₂P-Modified P-Doped Graphitic Carbon Nitride Hetero-Nanostructures for Efficient Photocatalytic Aqueous Cr (VI) Reduction. *Catalysts* **2023**, *13*, 437. [[CrossRef](#)]

Disclaimer/Publisher's Note: The statements, opinions and data contained in all publications are solely those of the individual author(s) and contributor(s) and not of MDPI and/or the editor(s). MDPI and/or the editor(s) disclaim responsibility for any injury to people or property resulting from any ideas, methods, instructions or products referred to in the content.